Acta Cryst. (1977). A33, 672–676

Electron-Optical Imaging of the Hollandite Structure at 3 Å Resolution

BY L. A. BURSILL and A. R. WILSON

School of Physics, University of Melbourne, Parkville, Victoria, Australia 3052

(*Received* 7 *December* 1976; *accepted* 24 *February* 1977)

This paper shows that it is possible markedly to improve the resolution obtainable in electron micrographs by deliberately using low beam divergence (2×10^{-4} rad) and by minimizing thermal spread in the electron gun. Point-to-point resolutions in the sub-3 Å range will be illustrated for the hollandite structure. Image matching, including the effects of both beam divergence and chromatic aberration, showed that the experimental images could be fitted using 2 Å objective aperture, with no divergence and defocus ripple of only 50 Å. In fact, these stringent experimental requirements must be met if useful structural information is to be obtained in the 2–3 Å range.

1. Introduction

O'Keefe & Sanders (1975) showed that the effective resolution obtained in electron micrographs is severely limited by the combined effect of spherical aberration and incident-beam divergence. For spherical aberration coefficient $C_s=1{\cdot}8$ mm and focused illumination (semi-cone angle 10^{-3} rad) the outer diffracted beams transmitted by the objective aperture do not contribute to the image. By matching experimental and computer simulated images with and without divergence they showed that the effective resolution was approximately 3·8 Å.

Fejes (1973) showed that chromatic aberration, in particular thermal spread in the electron gun, imposes a virtual ripple on the objective lens current. A defocus ripple of 250 Å was required to limit the resolution to 3·8 Å when good agreement with an experimental through-focal series, taken by Iijima, was obtained.

In this paper we show that it is possible to improve markedly the resolution by deliberately using low beam divergence (2×10^{-4} rad) and minimizing thermal spread in the electron gun.

2. Electron-optical requirements for imaging metal atoms in the hollandite structure

(*a*) *The hollandite structure*

Barium hollandite $BaMgTi_7O_{16}$ is a tunnel structure comprising a framework of stoichiometry MO_2 which encompasses large square tunnels (Fig. 1*a*). These contain Ba, which is coordinated to eight oxygens in the framework (Drysden & Wadsley, 1958). Analysis of the topological relationship between rutile, β-gallia, ramsdellite and hollandite led to the discovery of new types of intergrowth structures in the BaO–MgO–TiO_2 and BaO–Ga_2O_3–TiO_2 systems. In all these structures metal–metal spacings range upwards from 2·7 Å. The present paper reports a detailed analysis of the electron-optical requirements for locating the metal atoms in the simple hollandite structure, thereby serving as a basis for quantitative interpretation of our images of the intergrowth structures (Bursill, Netherway & Stone, to be published).

Hollandite is tetragonal with $a=10{\cdot}110$, $c=2{\cdot}986$ Å. Atomic coordinates are given by Drysden & Wadsley (1958). The space group is $I4/m$. Fig. 1(*b*) shows the metal atom positions projected along [001]. Characteristic metal–metal distances are Ba–Ba 7·2; Ti–Ti (corner-sharing) 3·2; Ti–Ti (edge-sharing) 2·7 Å. Thus the Ti–Ti distances are significantly less than the 3·8 Å spacings in the ReO_3-derived block and tunnel structures studied by Iijima & Allpress (1974). Fig. 1(*c*) shows the (001) reciprocal-lattice section with the corresponding *d* values. Clearly, in order to resolve the 2·7 Å Ti–Ti spacing the effective objective aperture must include beams out to 400. The apparent diameters of standard 40 and 60 μm objective apertures of the JEOL 100-C electron microscope are indicated on Fig. 1(*c*). We were therefore forced to use the 60 μm aperture, which included 45 beams, corresponding to theoretical resolution of 2·0 Å.

(*b*) *N-beam multislice images*

The physical basis of the multislice method of image calculation was explained by Goodman & Moodie (1974). A computer program using this basic theory has been developed in this laboratory. It is similar in principle to that of O'Keefe (1975) and Fejes (1973) but it incorporates a fast Fourier algorithm adapted to multislice calculations (MacLagan, 1975), whereby calculations involving up to 2049 beams may be completed in reasonable times. Three tests of the calculation were carried out.

(1) A unitarity test on the phase grating before it is multisliced, including the test of normalization to unity of the total transmitted intensity.

(2) After multislicing, the total intensity in all the beams was compared to unity to ensure that electrons were not being lost from the *N*-beam diffraction aperture.

(3) A convergence test for the image using increasing

numbers of beams in the diffraction aperture. This confirmed that the iteration was done with sufficiently large N (2049) and sufficiently thin slices (2 Å). It would also detect any truncation errors in the fast Fourier algorithm.

Fig. 2(*a*) to (*e*) shows a through-focal series calculated for 3·15 Å resolution, $C_s = 2{\cdot}4$ mm and crystal thickness 40 Å. The image oscillates rapidly with objective lens defocus Δf. Further calculations showed that a series of characteristic images occur which are stable for Δf ranges of approximately 70 Å. Furthermore, the image was very sensitive to small tilts ($\sim 6 \times 10^{-4}$ radian) away from the symmetrical [001] zone.

Fig. 3(*a*) to (*e*) shows the corresponding through-focal series assuming zero occupancy of Ba in the tunnels. Comparison of Figs. 2 and 3 will show that filled and empty tunnels should be distinguishable for all Δf values, but the difference is most directly interpretable for $\Delta f = -500$ to -600 Å. The filled tunnels show black blobs whereas the empty ones are white.

Calculations using Cs^{1+}, Cs^0, or Ba^{2+} in the tunnel sites gave through-focal series indistinguishable from Fig. 2.

(*c*) *Chromatic aberration*

The virtual defocus ripple of the objective lens may be taken as

$$\delta f_i = C_c[(\delta V/V)^2 + (2\delta i/i)^2]^{1/2}, \qquad (1)$$

where C_c is the chromatic aberration coefficient, $\delta V/V$ is the high-voltage stability, and $\delta i/i$ is the objective-lens current stability (Heidenreich, 1964). For the JEOL 100-C electron microscope used here $C_c \simeq 2{\cdot}0$ mm, $\delta V/V \simeq 10^{-6}$, $\delta i/i \simeq 2 \times 10^{-6}$ (manufacturers figures), yielding $\delta f_i = 45$ Å. A larger contribution to δf_i is expected to come from thermal spread in the electron gun. This may range up to 1 volt ($\delta V/V = 10^{-5}$), depending on the construction of the Wehnhelt cap, type of filament used, gun bias setting and emission temperature. Thus δf_i values up to approximately 200 Å could be expected.

Chromatic aberration was included in the calculation by taking a Gaussian weighted average of the image intensity over a range of defocus (Fejes, 1973). The wave amplitude was taken as

$$\psi_{H,\Delta f,C_s,C_c}(x,y) = \sum_{-m}^{+m} \frac{g(\Delta f - m\mathrm{d}f)}{2m+1} \sum_h \sum_k U_H(h,k) \times \exp\left[2\pi i \left\{\zeta(h,k)\left([\Delta f - m\mathrm{d}f] - \lambda C_s \zeta(h,k)\right) - \left(\frac{hx}{a} + \frac{ky}{b}\right)\right\}\right], \qquad (2)$$

where H is the crystal thickness (Å), Δf is the mean defocus, $\mathrm{d}f$ is the defocus sampling step size, m is the number of steps each side of Δf, g is the Gaussian weighting function, $U(h,k)$ is the amplitude of the diffracted beam h, k, $\zeta(h,k)$ is the excitation error for the beam h, k and a, b are the cell edges normal to the projection axis. We calculated over ± 2 standard deviations from the mean defocus. Fig. 4(*a*) to (*d*) shows the effect of increasing δf_i (taken as the standard deviation of the Gaussian) on a characteristic hollandite image (crystal thickness 40 Å, $C_s = 2{\cdot}4$ mm, 2 Å objective aperture, mean $\Delta f = -600$ Å). The image is significantly degraded for $\delta f_i > 100$ Å. Image calculations at 2·5 and 3·15 Å resolution, with no chromatic aberration, closely resembled the chromatically aberrated 2 Å calculation for $\delta f_i = 100$ or 200 Å but there was no precise one-to-one correspondence. In all cases the resolution was significantly better than the unaberrated 3·5 Å resolution image. Figs. 4(*e*), (*f*) show 3·15 and 3·5 Å images for $\Delta f = -600$ Å.

(*d*) *Beam divergence*

This was calculated by summing the image *inten-*

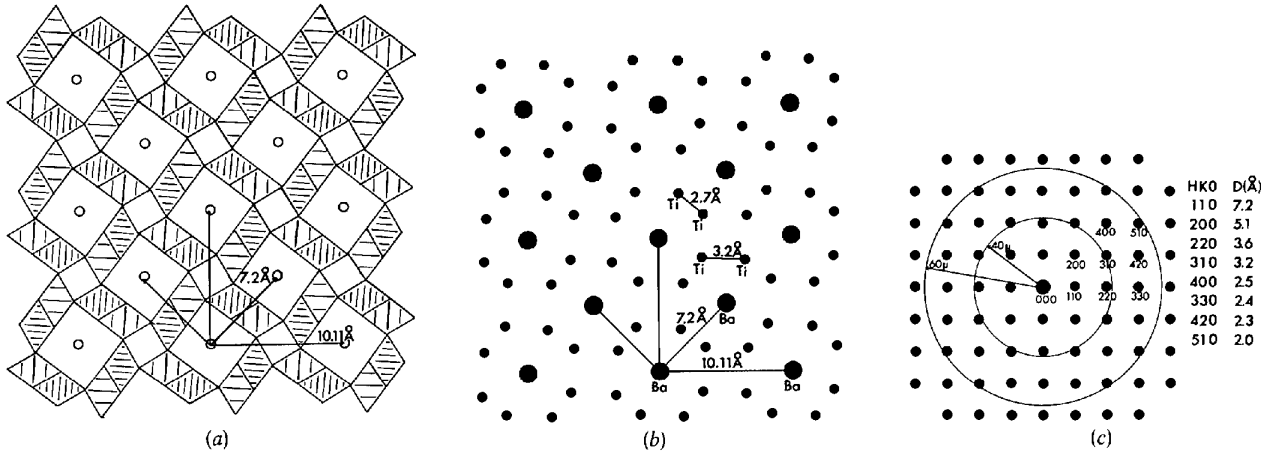

(*a*) (*b*) (*c*)

Fig. 1. (*a*) Crystal structure of hollandite, projected along [001]. (*b*) Metal atom positions projected along [001]. (*c*) (001) reciprocal-lattice section of hollandite; apparent diameters of 40 and 60 μm objective apertures, $hk0$ values and lattice spacings d_{hk0} are indicated.

sities for a range of crystal tilts covering the diffraction discs (O'Keefe & Sanders, 1975). This is time consuming as the iteration must be repeated for each tilt. Calculations using 9, 21 and 37 tilts simulated beam divergences of 6, 10 and 14×10^{-4} rad respectively. Since hollandite has a centre of inversion it was only necessary to use tilts in two quadrants. Unfortunately the line-printer output was incompatible with the fourfold axis of hollandite, preventing further symmetry reduction.

Fig. 5(*a*) to (*d*) shows the effect of increasing divergence on a characteristic image of hollandite ($H=$ 40 Å, $C_s=2{\cdot}4$ mm, $\Delta f=-200$ Å). Fine detail (~3 Å) is obliterated, even for the 6×10^{-4} calculation, 7·2 Å and occasionally 5 Å spacings now dominate the images. Clearly beam divergence less than 6×10^{-4} rad must be used if experimental images showing sub-3 Å spacings are to be obtained.

3. Experimental

(*a*) *Specimen preparation*

Preliminary observations were made using single crystals of Cs_xTiO_2 kindly provided by Dr J. C. Watts, CSIRO Division of Mineral Chemistry. Samples of stoichiometry $BaMgTi_7O_{16}$ were prepared by mixing high-purity $BaCO_3$, MgO and TiO_2 powders, pelletizing and heating at 800 to 1200°C for periods up to 14 days. A number of different superstructures of hollandite were found (Bursill, Netherway & Stone, in preparation). The following observations refer only to the crystal flakes showing the simple hollandite structure.

(*b*) *Objective pole-piece parameters*

Micrographs were taken using a slightly modified JEOL BLG top-entry goniometer. The specimen was lowered further into the pole piece than usual, giving objective lens current 1·6 A compared to the normal 1·15 A. Under these conditions we expect the focal length, chromatic aberration and spherical aberration parameters to be $f_0=2{\cdot}2$ mm, $C_c=2{\cdot}0$ mm, $C_s=2{\cdot}5$ mm. These figures were calculated with values provided by JEOL for an objective lens current of 1·45 A. A standard anticontamination device was used.

(*c*) *Micrographs*

Single-crystal fragments of hollandite were ground under chloroform in an agate mortar and pestle and deposited on carbon lace. Thin crystal flakes overlapping holes in the carbon film were tilted into the [001] zone and through-focal series recorded with the 60 μm objective aperture. Only the thinnest edges gave high-resolution images. The following images were all recorded with a standard hairpin filament and electron-optical magnification of 740 000×. Correction of objective-lens astigmatism was carried out at this magnification on the carbon support film. This was done by minimizing contrast at the appropriate degree of underfocus, then ensuring that streakiness did not appear on going through focus. This technique produces some difficulty as it is necessary to record images under zero-contamination conditions, *i.e.* where there is no carbon film. Consistent results were obtained provided the objective lens current did not alter significantly after astigmatism had been corrected on a piece of carbon film nearby. It is surprisingly difficult to correct astigmatism on the crystal image itself. The latter exhibits a series of images resembling a through-focal series for small changes in stigmator setting. These images all show high resolution and contrast which can only be distinguished from astigmatic images on comparison with computed images, when departures from correct symmetry occur.

Care was taken to ensure that the gun bias was not too small, so as to avoid unnecessary chromatic aberration due to thermal and space charge effects (Agar, Alderson & Chescoe, 1974).

Initially great difficulty was experienced in obtaining images showing 3 Å point-to-point detail. Whereas the 3·8 Å image of the block structure $Nb_{22}O_{54}$ was readily obtained with focused illumination (beam divergence 8×10^{-4} rad) most of the images of hollandite showed only 7 and 5 Å spacings (Fig. 6). One image was obtained from a crystal of Cs_xTiO_2 which showed fine detail on the 3 Å scale. The contrast was very sensitive to crystal tilt away from the symmetrically excited [001] zone (*cf.* areas *A* and *B* of Fig. 7). Thin edges of hollandite crystals are invariably flexible and although many crystals appear, from the selected area diffraction pattern, to have been symmetrically excited in fact only a small fraction of any one crystal flake proved to be so.

Following the above calculations we then deliberately reduced the beam divergence to 2×10^{-4} radians (Fig. 8*a*, *b*), when it proved possible to obtain 3 Å detail reproducibly. Fig. 9(*a*) to (*d*) shows four such images, taken at different degrees of underfocus. Exposures of up to 45 s were necessary, compared with 1 or 2 s for focused illumination. Comparison of Figs. 7 and 9 with Fig. 6 shows the remarkable increase in detail obtainable by simply reducing beam divergence. It is interesting to compare Figs. 7 and 9(*d*), which show contrast inside the hollandite unit cell. Fig. 7 shows much more detail, indicating very low divergence. The presence of some fine detail for the thinnest area of Fig. 6 suggests that the effect of divergence on resolution may be less important for very thin crystals (say <20 Å thickness).

4. Effect of spherical aberration on the through-focal series

C_s is included in the calculation *via* the reciprocal-space propagation function

$$P(h,k)=\exp\{-i\pi\lambda 4s^2[\Delta f+2C_s s^2\lambda^2]\}, \qquad (3)$$

where λ is the electron wavelength and

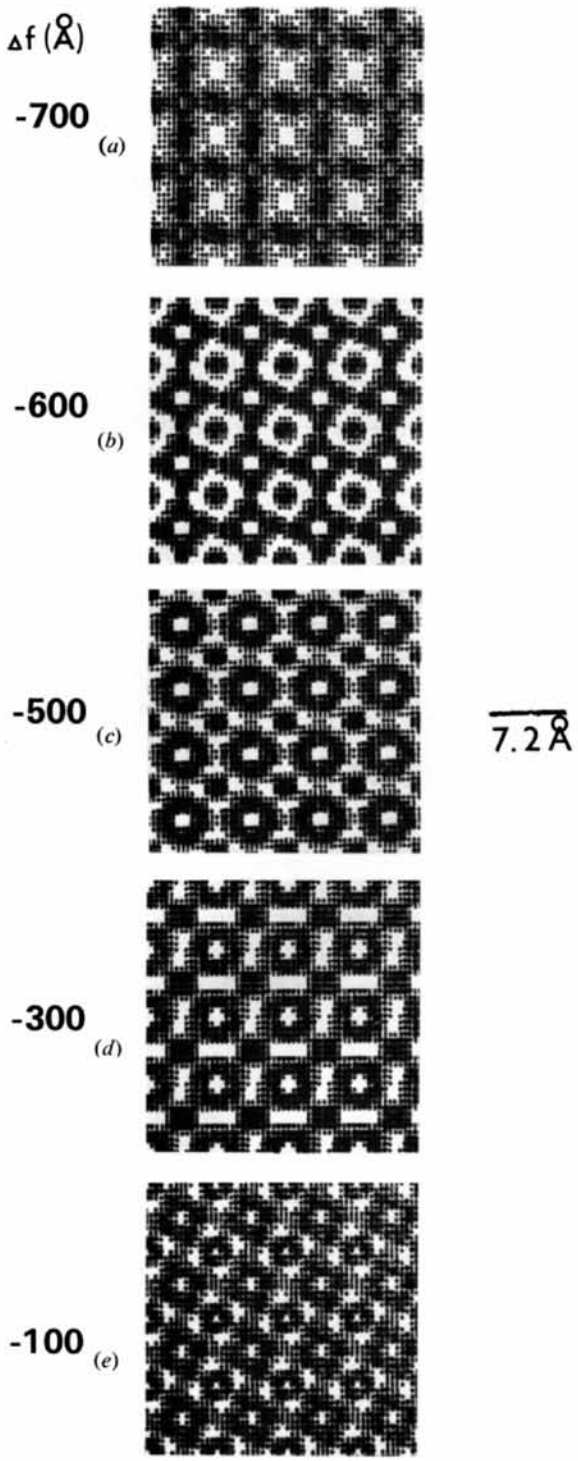

Fig. 2. (*a*) to (*e*). Through-focal series of hollandite, crystal thickness $H=40$ Å, $C_s=2{\cdot}4$ mm, resolution 3·15 Å.

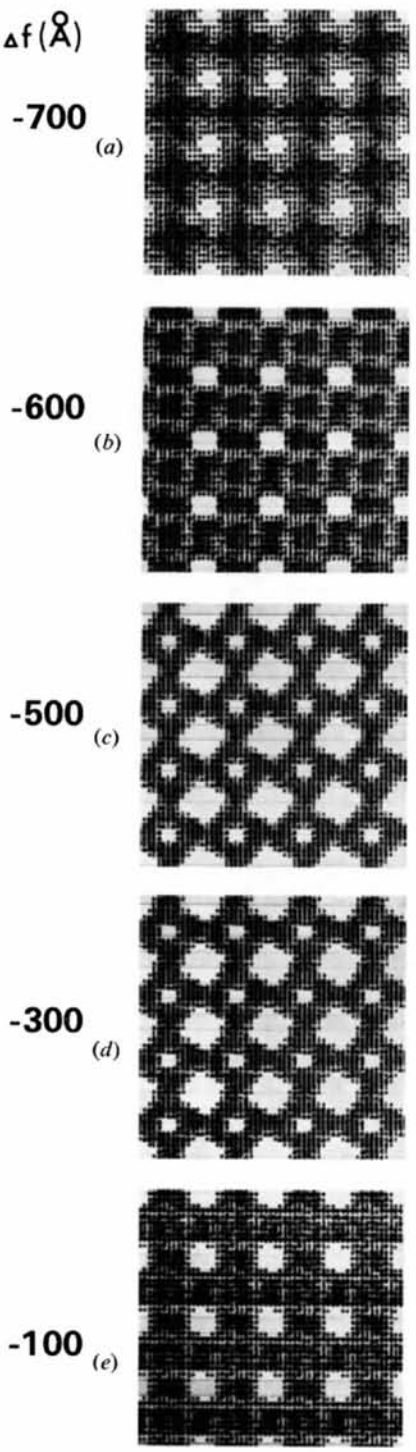

Fig. 3. (*a*) to (*e*) Through-focal series of hollandite framework, without Ba atoms, $H=40$ Å, $C_s=2{\cdot}4$ mm and resolution 3·15 Å. (Scale as Fig. 2.).

[*To face p.* 674

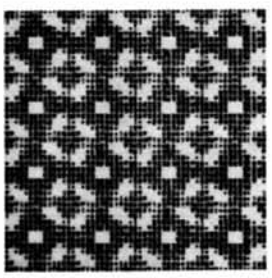

(*a*)

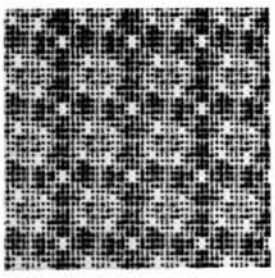

(*d*)

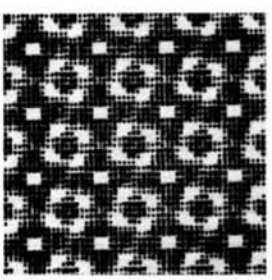

(*b*)

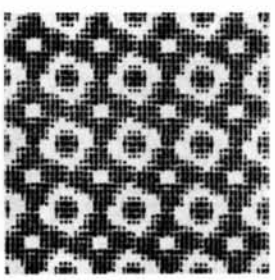

(*e*)

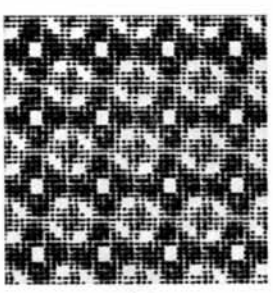

(*c*)

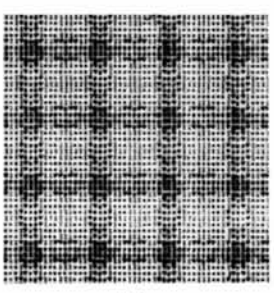

(*f*)

7.2 Å

Fig. 4. (*a*) to (*d*). Characteristic hollandite image ($H=40$ Å, $C_s=2{\cdot}4$ mm, resolution $=1{\cdot}99$ Å, $\Delta f=-600$ A) for increasing chromatic aberration; δf_i-0, 50, 100 and 200 Å for (*a*), (*b*), (*c*), (*d*) respectively. (*e*) Hollandite image, same as (*a*) except for resolution $=3{\cdot}15$ Å. (*f*) Hollandite image, same as (*a*) except for resolution $=3{\cdot}5$ Å.

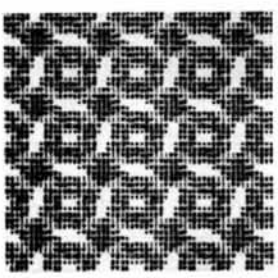

(*a*)

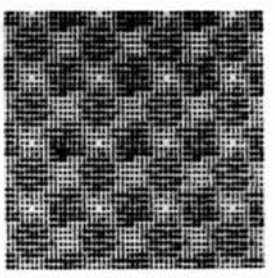

(*c*)

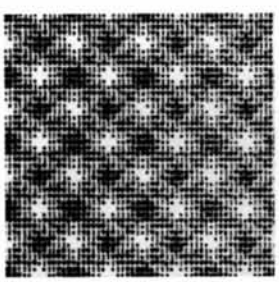

(*b*)

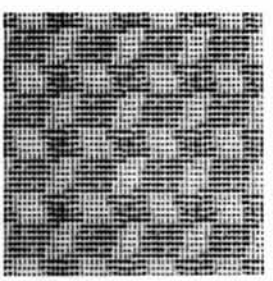

(*d*)

7.2 Å

Fig. 5. (*a*) to (*d*) Characteristic hollandite image ($H=40$ Å, $C_s=2.4$ mm, resolution $=1{\cdot}99$ Å, $\Delta f=-200$ Å) showing image degradation for increasing divergence [$0{,}6\times10^{-4}$, 10×10^{-4} and 14×10^{-4} rad for (*a*), (*b*), (*c*) and (*d*) respectively].

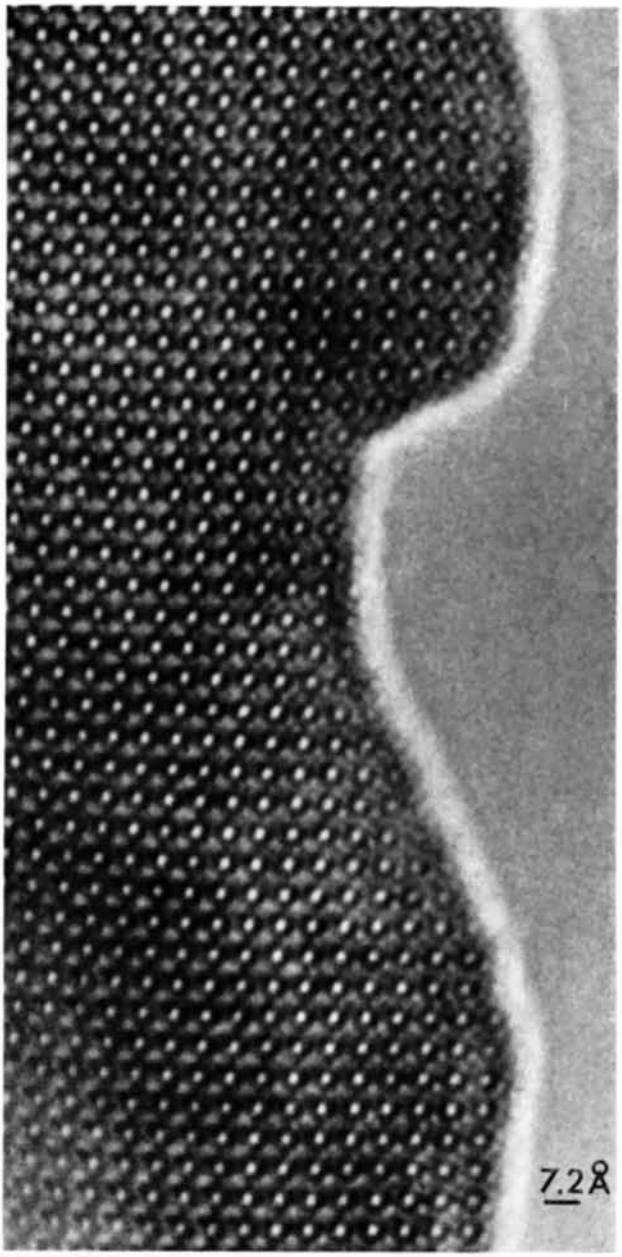

Fig. 6. Hollandite ($BaMgTi_7O_{16}$) image obtained with focused illumination. Note uniformity of contrast compared to Fig. 9 (*a*), (*b*), indicating that divergence has masked the effects on the image due to crystal flexure.

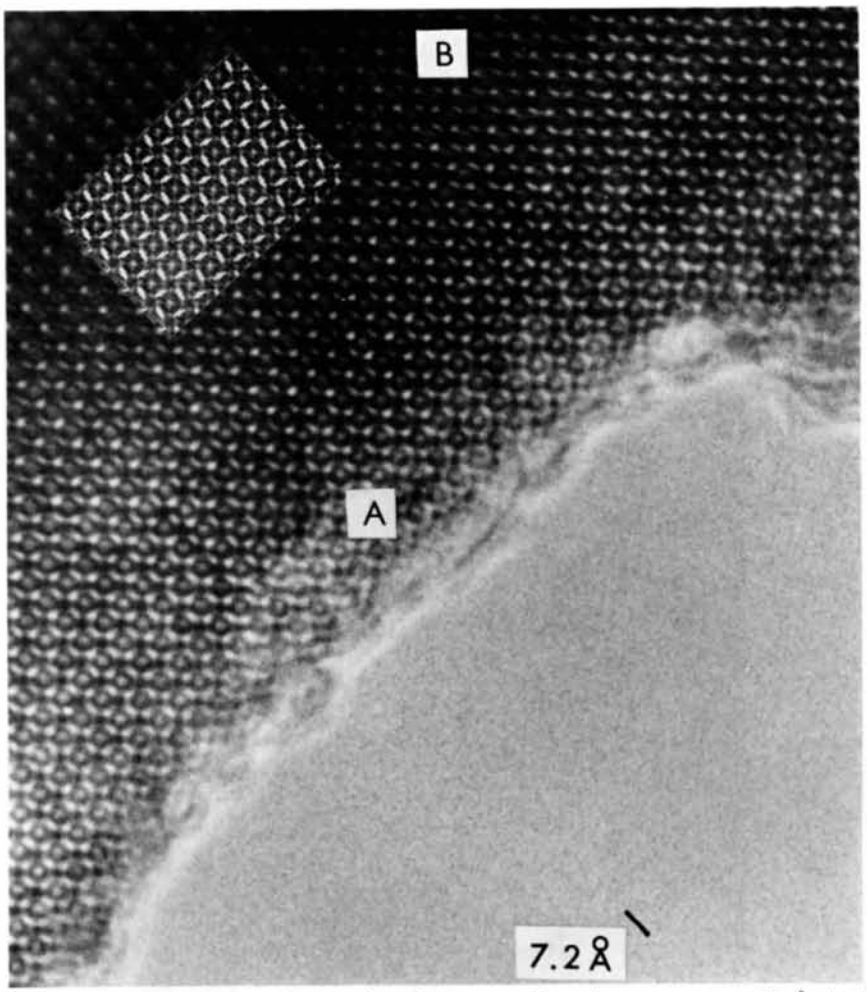

Fig. 7. Hollandite (Cs_xTiO_2) image obtained with very low divergence. Note the appearance of 3 Å detail and the variation in symmetry and detail of contrast as crystal bends away from [001] zone (*cf.* areas labelled *A* and *B*.

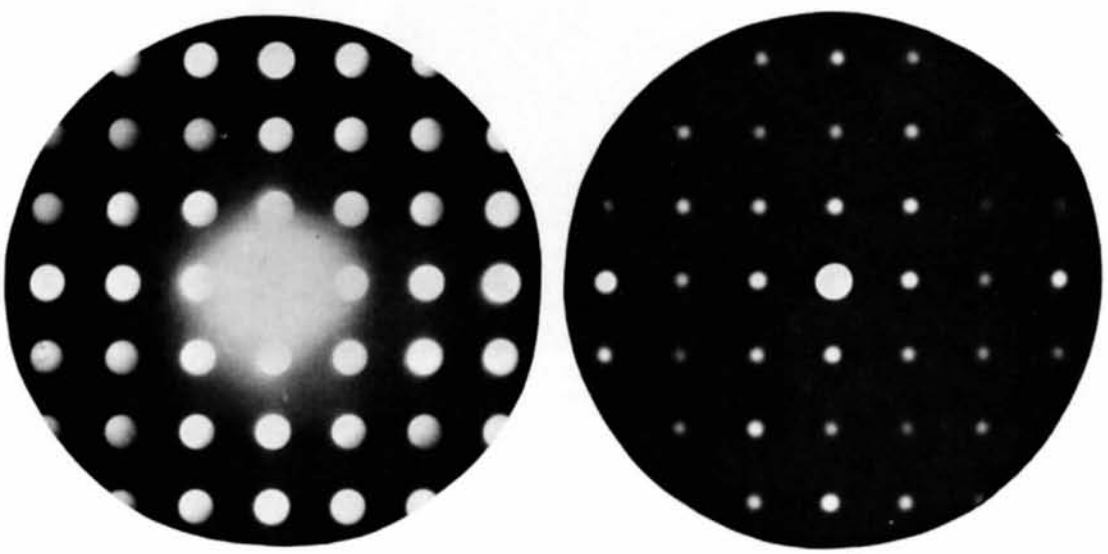

(*a*) (*b*)

Fig. 8. [001] diffraction patterns showing beam divergences of (*a*) 9×10^{-4} and (*b*) 2×10^{-4}.

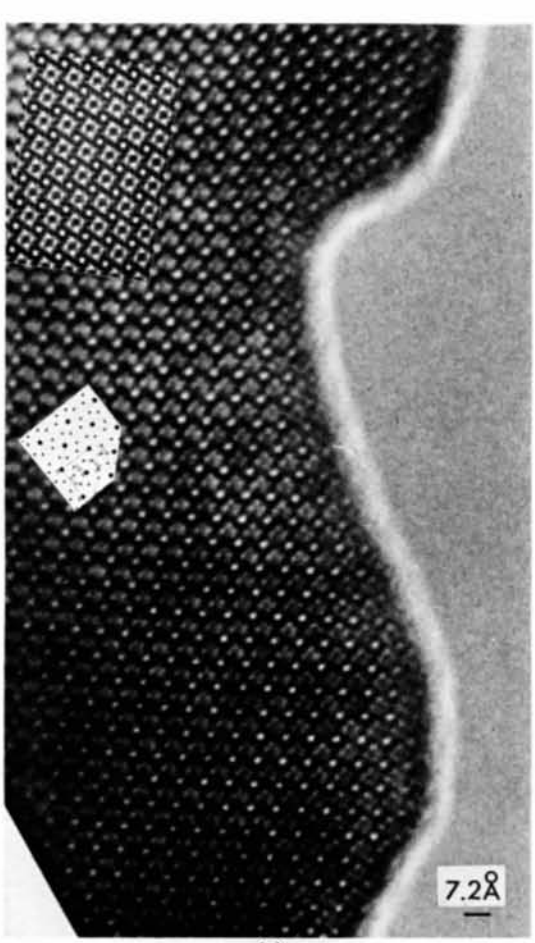

(*a*)

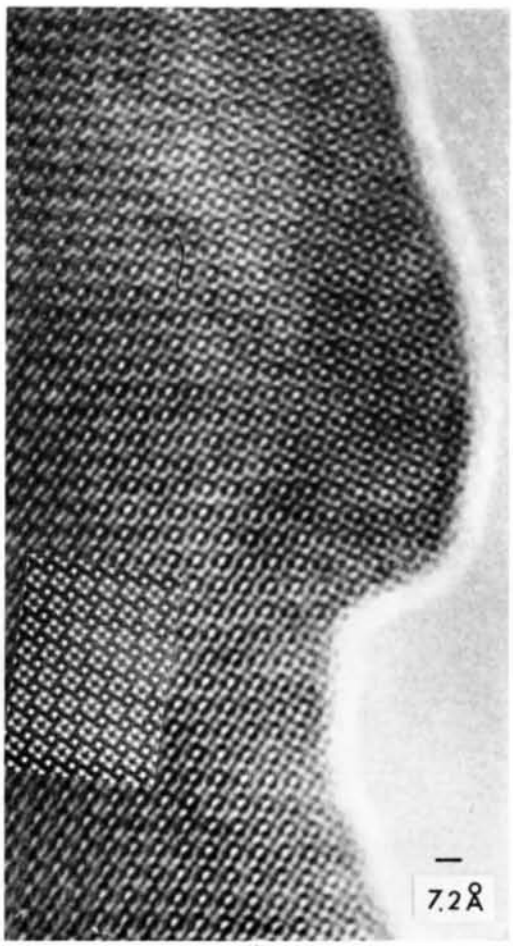

(*b*)

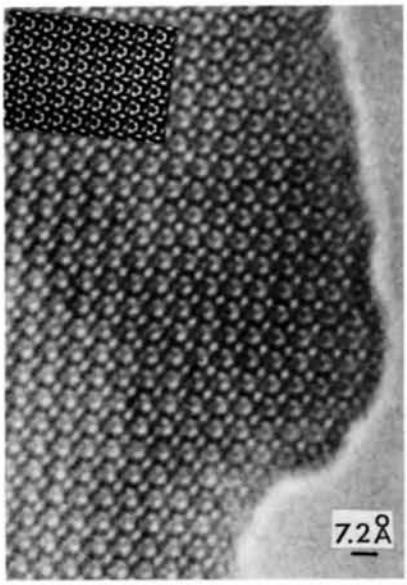

(*c*)

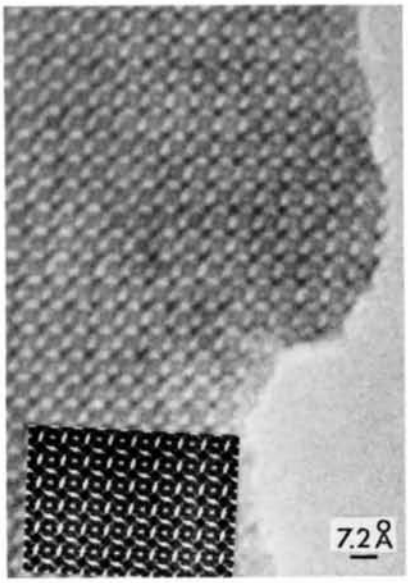

(*d*)

Fig. 9. (*a*) to (*d*). Part of a through-focal series of low-divergence images of hollandite ($BaMgTi_7O_{16}$) together with computer-simulated images. (*a*) also shows the location of metal atoms in the hollandite structure derived from the results of image matching. [The inset in (*a*) showing the metal atom positions is a reduction of Fig. 1 (*b*).] Note the remarkable increase in detail compared with Fig. 6, which shows the same area.

$$s = \sin\theta_B/\lambda = 1/2d_{hkl}\,.$$

The gross effect of a small increase in C_s is to shift the complete through-focal series in the direction of increasing underfocus. The magnitude of this shift is given very approximately by

$$\Delta f_s = -(\lambda C_s)^{1/2}/2 \qquad (4)$$

relative to the Gaussian image plane (Heinemann, 1971). Thus a through-focal series closely resembling Fig. 2 was obtained by using $C_s = 1{\cdot}8$ mm with Δf_s approximately 100 Å [*cf.* value of 71 Å predicted from equation (4)]. In order to determine C_s by image matching, or to confirm a calculated or manufacturer-supplied value, it is necessary to have an internal measure of Δf. This may be obtained by observing the behaviour of the Fresnel fringe at the crystal edge. A simple theory of the Fresnel fringe (Heidenreich, 1964) gives Δf in terms of the distance Δx_f of the first maxima from the crystal edge:

$$\Delta f = (\Delta x_f)^2/\lambda\,. \qquad (5)$$

This is quite accurate for $\Delta f \sim$ several 1000 but for small Δf it is essential to correct for spherical aberration. Introduction of the latter means that the Fresnel fringe never disappears completely, at any Δf. Instead we obtain a minimum contrast condition for $\Delta f = \Delta f_s$ given by equation (4) above. We may therefore write Δf in terms of Δx_f and C_s as follows

$$\Delta f = \pm(\Delta x_f)^2/\lambda - (\lambda C_s)^{1/2}/2\,, \qquad (6)$$

where the + and − signs refer to over and under focus respectively. Thus the position of minimum contrast should appear at approximately $\Delta f = -470$ Å for $C_s = 2{\cdot}4$ mm. Using equation (6) we may therefore assign rough values for Δf to the experimental images, as shown in Table 1.

Table 1. *Δf values deduced from equation (6) and best-fit computed images*

	Δx_f (Å)	Δf (equation 6)	Δf computed image
Fig. 7	~ −2	−320	−200
Fig. 9(*a*)	~5	−1150	−1160
Fig. 9(*b*)	~5	−1150	−1120
Fig. 9(*c*)	~2·5	−640	−600
Fig. 9(*d*)	~ −2	−320	−200

5. Image matching

A large number of through-focal series were computed, for different crystal thicknesses, spherical aberrations, chromatic aberrations and divergences. The best-fit computed images are shown in Fig. 7 and Fig. 9(*a*), (*b*), (*c*), (*d*). These were obtained for $H = 40$ Å, $C_s = 2{\cdot}4$ mm, $\delta f_i = 50$ Å and zero divergence. The resolution used in the calculations was 1·99 Å, as determined by the size of the objective aperture. Δf values deduced from the computed micrographs are given in Table 1. These agree fairly well with those calculated from equation (6), considering that it is difficult to measure Δx_f accurately. Thus the value $C_s = 2{\cdot}4$ mm deduced by image matching is very close to the value 2·5 mm deduced from the figures supplied by JEOL. For more accurate determination of C_s using image matching it will be necessary to compute the Fresnel fringe contrast accurately and match this to the experimental images. Preliminary calculations using the method of periodic continuation confirm the above value.

To obtain good agreement with Fig. 9(*c*) it was necessary to include a small beam tilt (centre of Laue circle at $h,k = -0{\cdot}187,\ 0{\cdot}050$) corresponding to a tilt of 6×10^{-4} rad in the calculation. Note that the detail of the experimental image often varies from one unit cell to the next. These variations are most simply explained in terms of flexure of the thin edges. There is no evidence for the occurrence of completely empty tunnels at random, as proposed by Drysden & Wadsley to account for variable stoichiometry of the hollandite phase. Ordered superstructures of hollandite will be the subject of another publication.

6. Conclusion

The good agreement between experimental and computed images demonstrates that point-to-point resolutions in the sub-3 Å range have been achieved. Fig. 7 and Fig. 9(*b*) especially show better agreement with the 2 Å calculation ($\delta f_i = 50$ Å) than with either 2·5 or 3·15 Å calculations ($\delta f_i = 0$), because of the especially low divergence used.

It is possible to locate all the metal atoms in the [001] projection of hollandite. This is illustrated, for example, in Fig. 9(*a*) where the interpretation of the contrast is more direct. The Ba atoms image as a black blob in the centre of a large square, representing the large occupied tunnel. Titanium and magnesium in octahedral sites image as a black square surrounding a bright blob representing the small empty tunnel in the rutile-like columns of the hollandite framework.

We thank Dr A. E. C. Spargo for valuable discussion and encouragement, the Australian Research Grants Committee for financial support, and Dr J. C. Watts for providing the single crystals of Cs_xTiO_2. One of us (ARW) acknowledges the financial assistance of an Australian Postgraduate Research Award.

References

AGAR, A. W., ALDERSON, R. H. & CHESCOE, D. (1974). *Principles and Practice of Electron Microscope Operation*, pp. 15–21. Amsterdam: North-Holland.

DRYSDEN, J. S. & WADSLEY, A. D. (1958). *Trans. Faraday Soc.* **54**, 1574–1580.

FEJES, P. (1973). PhD Thesis, Arizona State Univ.

GOODMAN, P. & MOODIE, A. F. (1974). *Acta Cryst.* A**30**, 280–290.

HEIDENREICH, R. D. (1964). *Fundamentals of Transmission Electron Microscopy*, p. 112. New York: Interscience.
HEINEMANN, K. (1971). *Optik*, **34**, 113–128.
IIJIMA, S. & ALLPRESS, J. G. (1974). *Acta Cryst.* A**30**, 22–36.
MACLAGAN, D. S. (1975). MSc Thesis, Univ. of Melbourne.
O'KEEFE, M. A. (1975). PhD Thesis, Univ. of Melbourne.
O'KEEFE, M. A. & SANDERS, J. V. (1975). *Acta Cryst.* A**31**, 307–310.

Acta Cryst. (1977). A**33**, 676–677

Polytypisme du Carbure de Silicium: Localisation et Structure du Polytype 102*R* Basé sur la Séquence (34)

PAR JEAN-PIERRE GAUTHIER ET PIERRE MICHEL

Université Claude Bernard Lyon I, *Laboratoire de Minéralogie–Cristallographie, Associé au CNRS* (*ERA* 600), 43 *boulevard du* 11 *Novembre* 1918, 69621 *Villeurbanne, France*

(*Reçu le* 14 *janvier* 1977, *accepté le* 10 *mars* 1977)

Reflexion electron diffraction (RHEED) patterns have been made on a SiC crystal fracture, showing a 102*R* polytypic modification on a 6*H* matrix. Its Zhdanov sequence can be written as $|(34)_4 33|_3$. The transition between 6*H* and 102*R* polytypes appears rather complex and can be explained with some typical diagrams.

Introduction

Une récente revue (Trigunayat & Chadha, 1971) récapitule l'ensemble des polytypes connus du carbure de silicium. Ces auteurs rappellent le fait empirique que, dans la notation de Zhdanov, seuls les nombres 2, 3 et 4 apparaissent, exception faite du nombre 5 pour le polytype $24R_1$ noté $(53)_3$ (Gomes de Mesquita, 1965) et du nombre 6 pour le polytype 174*R* noté $|(33)_3 6(33)_5 4|_3$ (Tomita, 1960). De plus, le nombre 4 est peu fréquent et s'introduit en général comme un accident 34 ou 43 dans une séquence régulière 33, comme par exemple dans le 39*R*: $(3334)_3$ ou le 111*R*: $|(33)_5 34|_3$. Jusqu'à la découverte du polytype 189*R* (Ram, Dubey & Singh, 1973) aucune structure polytypique n'était formée à partir de la séquence 34 du polytype de base 21*R*. Dans ce polytype 189*R* noté $|(34)_8 43|_3$, le dernier groupement 43 apparaît comme un 'retournement' de la séquence 34.

Nous venons de mettre en évidence, par diffraction électronique par réflexion, selon une méthode d'investigation récemment décrite (Michel, Gauthier & Riwan, 1976) un nouveau polytype rhomboédrique à 102 couches basé sur la séquence 34, prévu depuis longtemps (Verma & Krishna, 1966), mais non encore observé.

Diagrammes obtenus

Ce polytype a été repéré initialement sur un cliché de diffraction par des traînées de réflexion perpendiculaires à l'axe d'empilement *c*, à l'intersection d'une zone de Laue (Fig. 1*a*). L'excitation perturbatrice de certaines de ces traînées par des lignes de Kikuchi de surstructure ne masque cependant pas les renforcements d'intensité du type 21*R*: sept intervalles principaux peuvent être décomptés dans la séquence.

Une recherche plus approfondie et une orientation judicieuse du cristal ont permis d'obtenir des diagrammes de pseudo-réflexion sur toute sa section, lorsqu'on le déplace dans la direction **c**, normale à la face de base. Ce cristal présentait le faciès classique des cristaux fabriqués en four industriel, avec une large face plane du type (0001) et, à son opposé, une surface convexe sans plans cristallographiques apparents, et des faces latérales correspondant aux forms hexagonales du prisme et de la pyramide.

Une fracture a été réalisée perpendiculairement au plan de base, et la partie convexe de la cassure a été soumise au faisceau électronique.

Si l'on prend comme direction positive la normale sortant de la face plane (Fig. 2*a*), l'exploration du cristal a donné, d'arrière en avant, quatre types principaux de clichés. Nous présenterons seulement les rangées $|10l|^*$ des plans réciproques a^*c^* enregistrés sur plaques photographiques. (α) Un cliché obtenu sur une zone d'épaisseur millimétrique correspondant au polytype simple 6*H* (Fig. 1*b*). (β) Un cliché présentant des traînées continues avec renforcements d'intensité du type 6*H*. La zone touchée s'étend sur environ 250 μm et correspond, soit à un désordre partiel de la matrice, soit à un ou plusieurs polytypes à très longue

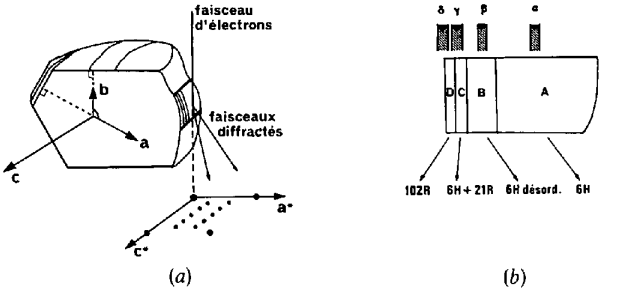

(*a*) (*b*)

Fig. 2. (*a*) Aspect classique d'un cristal de SiC. Positionnement de la fracture par rapport au faisceau électronique. (*b*) Section du cristal au voisinage de l'impact du faisceau. Positions α, β, γ, δ du faisceau par rapport aux zones polytypiques *A*, *B*, *C*, *D*.